GEOPHYSICAL RESEARCH LETTERS, VOL. 27, NO. 5, PAGES 637-640, MARCH 1, 2000

Global multispectral auroral imaging of an isolated substorm

S. A. Cummer,[1,2] R. R. Vondrak,[1] N. Østgaard,[3] J. Stadsnes,[3] J. Bjordal,[3] D. L. Chenette,[4] M. J. Brittnacher,[5] G. K. Parks,[5] J. B. Sigwarth,[6] L. A. Frank [6]

Abstract. We analyze simultaneous visible, ultraviolet (UV), and X-ray auroral images of an isolated substorm on January 25, 1998. The total precipitating electron energy flux and mean energy extracted near substorm maximum from each of the imagers are in acceptable agreement. The expansion phase visible, UV, and X-ray emissions are morphologically similar, with the brightest emissions coming from the auroral surge. However, during the recovery phase, there are regions of bright X-ray emissions near local midnight and dawn that do not correspond to obvious features in the visible and UV images. X-ray energy analysis in these regions reveals a high energy (~30–100 keV) component of the precipitating electron population that contributes ~30% of the total electron energy flux. The temporal development of the X rays indicates that the dawn emissions originate in a drifting electron population, while the newly revealed midnight emissions originate in a continuous injection of energetic electrons in a narrow local time region.

Introduction

The auroral substorm was first discovered from a careful synthesis of ground-based all-sky auroral images [*Akasofu*, 1964]. With the advent of space-borne auroral imaging, it became possible to view a large portion of the auroral oval nearly simultaneously and thereby to study global substorms individually rather than statistically. The auroral imager on the Dynamic Explorer 1 (DE-1) spacecraft was the first to provide global auroral images (with 12 min time resolution) over a period long enough to study an individual substorm from onset to recovery [*Craven and Frank*, 1985].

The suite of imagers on the Polar spacecraft offers a unique opportunity to study individual substorms globally and simultaneously at visible, ultraviolet (UV), and X-ray wavelengths. Simultaneous multispectral imaging shows the dynamics of different particle populations involved in the substorm process and enables detailed quantitative measurements of the electron energy flux into the ionosphere. To utilize the capabilities of multispectral imaging, we searched for a relatively isolated substorm that was viewed nearly in entirety by the three imagers. Such an event occurred on January 25, 1998 between 0350 and 0530 UT, and we present a subset of the simultaneous images from the three instruments which show the temporal development of the substorm at different wavelengths. The emissions vary differently with local time during the expansion and recovery phases, and we assess the origin of precipitating high energy (~30–100 keV) electrons responsible for the differences. We find reasonably good agreement between the total precipitating electron energy flux and average energy derived from the images at different wavelengths.

[1]Laboratory for Extraterrestrial Physics, NASA Goddard Space Flight Center, Greenbelt, Maryland

[2]Now at Department of Electrical and Computer Engineering, Duke University, Durham, North Carolina

[3]Department of Physics, University of Bergen, Bergen, Norway

[4]Lockheed Martin Advanced Technology Center, Palo Alto, California

[5]Department of Geophysics, University of Washington, Seattle, Washington

[6]Department of Physics and Astronomy, University of Iowa, Iowa City, Iowa

Paper number 1999GL003678.
0094-8276/00/1999GL003678$05.00

Instruments

On January 25, 1998, the Visible Imaging System (VIS) Low Resolution Camera (LRC) sequentially acquired auroral images at wavelengths of 557.7 nm, 391.4 nm, and 630.0 nm with 44 second integration times and with a spatial resolution of ~20 km. The Ultraviolet Imager (UVI) continuously acquired images of the Lyman-Birge-Hopfield long (LBHl, ~160–180 nm) emissions with a 36.8 second integration time. The UVI spatial resolution is nominally ~30 km, but the wobble of the Polar despun platform degrades this resolution somewhat in one dimension. The Polar Ionospheric X-ray Imaging Experiment (PIXIE) detected 2.5–9.1 keV (low energy) X-rays for 5 min out of every 10 and continuously detected 7.6–20.7 keV (high energy) X-rays. We have assembled the X-ray counts into images with 5 and 10 min integration times for low and high energy ranges, respectively. The spatial resolution of PIXIE image plane is ~150 km at the spacecraft altitude for this event, but the images are further blurred by a uniform pinhole aperture size equivalent to ~600 km. During this period, the PIXIE field of view (FOV) covers the entire auroral oval, while the VIS LRC and UVI FOVs cover approximately 1600–0500 MLT and 1600–0700 MLT, respectively.

Images from January 25, 1998

This substorm began between 03:53:14 and 03:53:50 UT, as determined from the UVI LBHl image showing the first discernible brightening in the onset region. Figure 1 shows the simultaneous VIS 557.7, UVI LBHl, and PIXIE low and high energy X-ray images over the course of the substorm. Due to the fundamental differences between X-ray and visible/UV photon production, the absolute brightness of the X ray aurora is much lower than that of the UV and visible aurora (1 R=$10^6/4\pi$ photons cm^{-2} s^{-1} sr^{-1}). Each image is labeled with its integration time. We show images representative of different stages in the substorm development or containing features of interest. The individual images are shown on uniform clockdial grids as a function of corrected geomagnetic (CGM) latitude and local time.

The emissions at 0403 UT, shortly after substorm onset, are bright in the VIS and UVI images, and are visible but weak in the PIXIE high and low energy images. By 0411 UT, when the westward traveling surge has developed (as seen in the VIS image at 2100 MLT) and the emissions have expanded eastward, the X-ray emissions are much brighter and are centered about a region that is about one hour of local time to the east of the westward surge. At 0423, the low and high energy X-ray emissions peak in brightness at 2100–2200 MLT and 0000–0100 MLT, respectively. In the

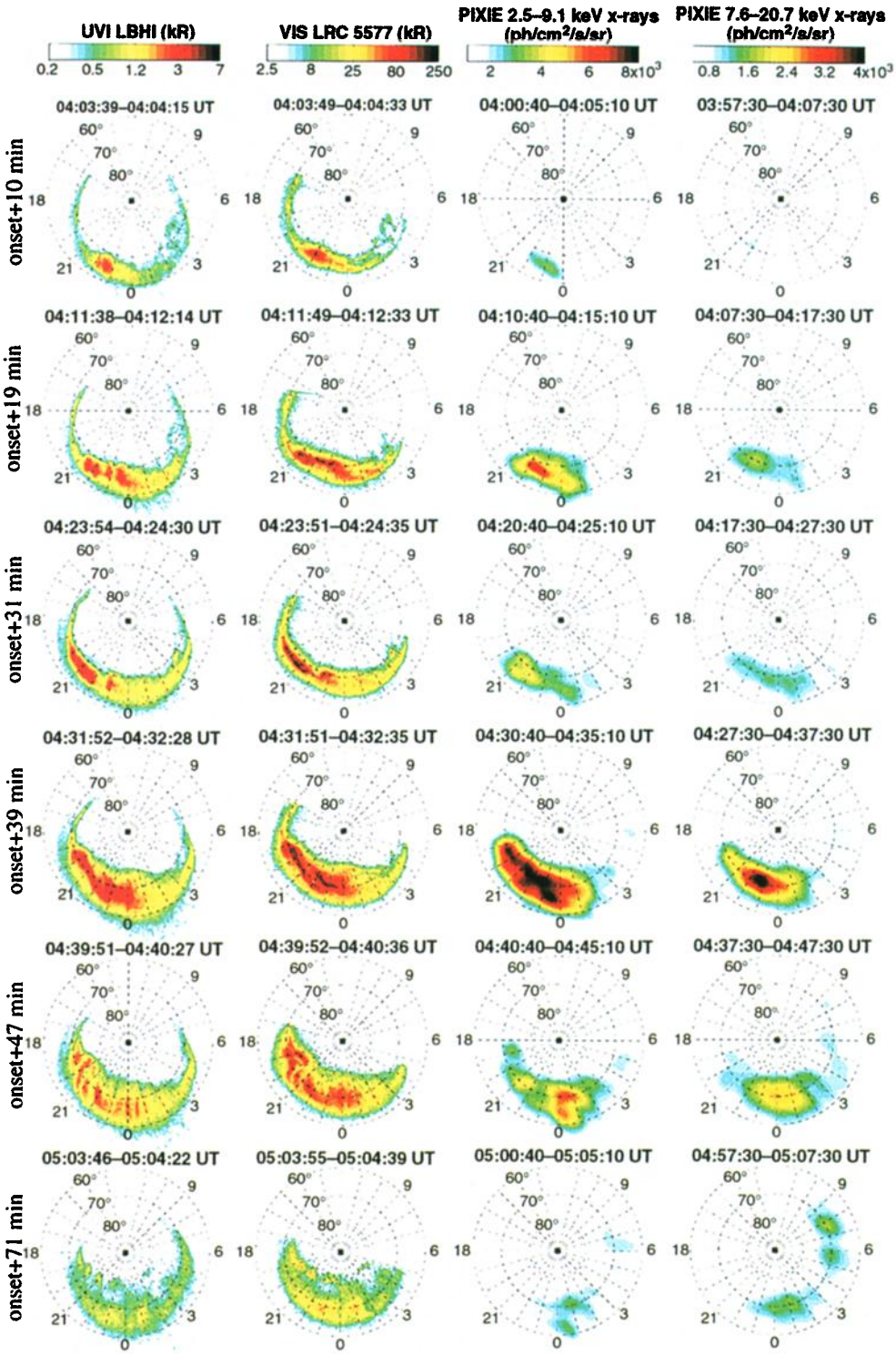

Figure 1. An auroral substorm on 25 January 98 as seen simultaneously in ultraviolet, visible, and X-ray wavelengths. Substorm onset was at 0353 UT. The images are displayed on a CGM clockdial grid and are each labeled with their integration time.

VIS and UVI images, these regions correspond to a region just east of the surge and a region of diffuse emissions at the equatorward edge of the auroral oval. Given the known high energies (often >5 keV) of surge-associated electrons, these X-ray emissions from the surge region are expected. The east-of-surge equatorward emissions and local morning emissions later in the substorm have been interpreted as resulting from the precipitation of electrons accelerated at substorm onset that undergo eastward gradient and curvature drift along lines of approximately constant L value [*Craven and Frank*, 1985; *Anderson et al.*, 1998; *Østgaard et al.*, 1999a]. The substorm underwent a second intensification at 0431 UT. CANOPUS magnetometer data (not shown) confirms the presence of two distinct intensifications in this substorm. The brightest emissions at all wavelengths are between 2200 and 2300 MLT and are as-

sociated with discrete auroral structures clearly visible in the VIS image. The substorm began to decay by 0440 UT with a reduction in all emission intensities. The emissions continue until approximately 0530 UT.

Over the course of the substorm, the UVI LBHl and VIS 557.7 nm emissions are generally similar. This is to be expected, as the LBHl emission intensity is proportional to the total precipitating electron energy flux [*Germany et al.*, 1994], and the 557.7 nm brightness depends only weakly on electron energy [*Rees et al.*, 1988]. However, in the recovery phase after 0440 UT, the X-ray and visible emissions differ substantially. The X-ray images are brightest between 0000 and 0200 MLT, but the VIS and UVI images are almost uniformly bright between 1900 and 0200 MLT and show no hint of this brighter region. Also, at 0505 UT, a bright high energy X-ray emission region appears between 5 and 0800 MLT which remains visible until ~530 UT. This feature is outside the FOV of UVI and VIS, but *Østgaard et al.* [1999a] showed that it is usually not distinct in UVI images. Since the low and high energy X-ray images are produced by electrons with energies >2.5 and >7.6 keV, respectively, the regions where the X-ray and UV or visible emissions differ most significantly are regions of either high ($\gtrsim$10 keV) and low ($\lesssim$2.5 keV) energy electron precipitation. These differences are analyzed in more detail in the following sections.

Precipitating Electron Energy Analysis

The multispectral capabilities of the individual Polar imagers enable detailed quantitative remote sensing of the precipitating electron spectrum. All three imagers can provide measurements of total precipitating electron energy flux, and PIXIE and VIS are operated in modes which can assess mean electron energy. To convert the images to electron energy flux, we assume UVI LBHl emissions of 120 R erg^{-1} cm^2 s [*Germany et al.*, 1994] and VIS 391.4 nm albedo-corrected emissions of 400 R erg^{-1} cm^2 s. The latter quantity is determined from 427.8 nm emission simulations [*Strickland et al.*, 1989] and by assuming a fixed ratio of 391.4 to 427.8 nm emissions of 3.5 [*Rees et al.*, 1988]. The mean electron energy is extracted from the intensity ratio of the VIS 630.0 nm and 391.4 nm images as described by *Strickland et al.* [1989], who assume a modified maxwellian form for their standard electron distribution for which the mean energy is approximately 1.7 times the maxwellian characteristic energy when averaged over energies from 0.1 to 100 keV. We cannot calculate average energy with UVI data for this period because the instrument only acquired LBHl images.

To extract the electron energy spectrum from the observed PIXIE X-rays, we find the single or double exponential electron energy spectrum whose calculated bremsstrahlung spectrum best matches the observed X-ray spectrum in 6 energy channels, using the technique described by *Østgaard et al.* [1999b]. A double exponential electron spectrum generally produces a better fit to the wide energy range (~3–20 keV) of the observed X-rays. *Anderson et al.* [1998] analyzed a narrower X-ray energy range by assuming a single exponential electron spectrum and found that the inferred energy flux and mean energy agreed well with observed <30 keV electrons.

From the exponential fit we can calculate the total precipitating electron energy flux for energies $\gtrsim$3 keV (PIXIE is not sensitive to X-rays produced by electrons with energy <2.5 keV) and mean energy over the range 0.1 to 1000 keV. This reduction to a single energy parameter tends to obscure the information contained in the higher energy exponential which can contribute significantly to ionization at lower altitudes (<120 km). Thus, to emphasize this high energy precipitation, we also display the mean energy of this second exponential where it is found in the PIXIE data.

In Figure 2, we compare the energy flux and mean energy measurements from the images at 0440–0445 UT. The VIS and UVI

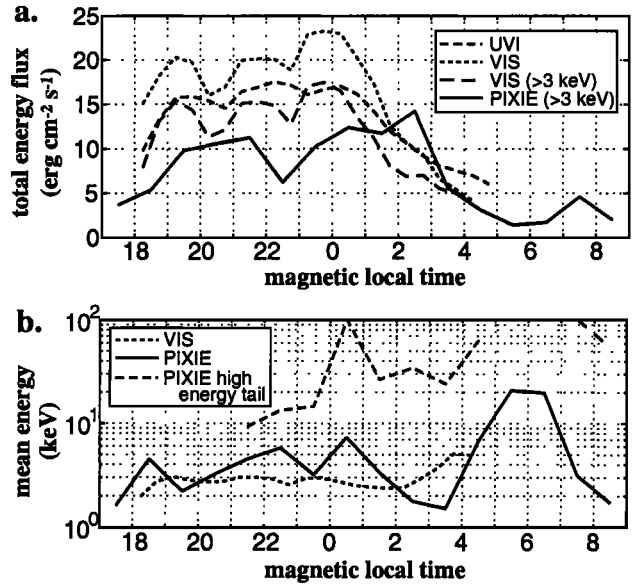

Figure 2. Energy parameters extracted from the three imagers between 0440 and 0445 UT. a: Total energy flux as a function of local time. b: Mean electron energy and high energy tail e-folding energy as a function of local time.

parameters are the values of peak brightness in 0.5 hour local time bins after a 750 km diameter spatial averaging. The PIXIE emissions were averaged over 8 degrees of magnetic latitude centered at 70° magnetic latitude (MLAT) and over 1 hour of MLT. Since the peak X-ray emissions are approximately centered about 70° MLAT, these spatial averaging methods are essentially equivalent. Figure 2a shows the total precipitating electron energy flux measured by each of the three imagers as a function of MLT, while Figure 2b shows the mean energy calculated from the VIS and PIXIE observations. The presence of the higher energy exponential, where found from the PIXIE data, indicates the presence of a high energy tail to the electron distribution. This high energy exponential contains ~30% of the total precipitating electron energy flux detected by PIXIE in the post-midnight region. The agreement between the calculated energy fluxes is generally good, with a mean deviation between the VIS and UVI measurements of total energy flux of ~25%, and a mean deviation between the PIXIE and VIS >3 keV energy fluxes of ~40%. The mean deviation between the VIS and PIXIE mean energies is ~50% at local times before 0400 MLT, where the auroral oval was within the VIS field of view. Given the known uncertainties in relating electron precipitation and auroral emissions [*Robinson and Vondrak*, 1994], these measurements are in acceptably good agreement. The observed X-ray counts result in uncertainties in the derived parameters of ~30% near midnight (where the counts are relatively high) and ~60% near dawn (where the counts are lower). Uncertainties in the UVI data and analysis lead to standard deviations in the derived parameters of ~40% [*Germany et al.*, 1997]. We expect similar uncertainties in the VIS energy flux and mean energy due to uncertain parameters in the interpretive model [*Strickland et al.*, 1989].

High Energy Precipitation

The origin of the high energy electrons seen by PIXIE is revealed by an analysis of the substorm image sequence. Figure 1 shows that there are two distinct recovery phase high energy X-ray emission regions. One region, between 0500 and 0800 MLT, contains emissions that are strongest during 0447–0507 UT, which is 20–30 min after the strongest substorm intensification. This region has been previously examined by *Østgaard et al.* [1999a; 1999b], who

found from a number of substorms that this delay corresponded to the expected drift times for $\gtrsim$90 keV electrons originating at substorm onset. The data presented here support this interpretation, as 100 keV electrons injected at the substorm intensification at 0430–0435 UT and 2200–2300 MLT would drift approximately 4 hours of local time in 10 min of real time [*Østgaard et al.*, 1999a] and thereby arrive at 0600–0700 MLT at the observed time of 0450 UT. An answer to the related question of why these drifting electrons are preferentially precipitating near 0600–0700 MLT has been suggested in the context of wave-particle interactions [*Jentsch*, 1976]. The statistical observations of peaks near 0600 MLT in both 30 keV to 2.5 MeV electron precipitation seen by NOAA-TIROS satellites [*Codrescu et al.*, 1997] and ELF wave power at geosynchronous altitude seen by GEOS 2 [*Parrot and Gaye*, 1994] support this view.

The newly revealed second region of high energy X-ray emissions (and thus precipitation of high energy electrons) is between 0000 and 0200 MLT. While such emissions are expected at substorm onset from the injection of energetic electrons, the images from 0417 to 0457 UT (some of which are in Figure 1) show an X-ray emission peak that persists through substorm recovery phase. Energy analysis of the X-ray data show the presence of a $\sim$100 keV population from 0417 to 0447 UT, with the energy dropping to 12 keV by 0457 UT. For such an energetic population to last for 30 min in one location requires that the electrons be continuously supplied at that local time due to their fast gradient and curvature drift. This indicates that, for this substorm, the process responsible for accelerating electrons in the magnetotail to $\sim$100 keV energies and sending them earthward operates on time scales approaching 30 min. Whether the morphology and duration of this high energy precipitation is a common feature of substorms is a subject for further study.

Conclusions

We have presented an analysis of simultaneous and global auroral images of an isolated substorm at visible, UV, and X-ray wavelengths that reveals some new features of large scale auroral emissions. The UV and visible emissions are generally similar, with the brightest emissions coming from auroral surge structures in the premidnight sector. The brightest expansion phase X-ray emissions come from the same regions, reflecting the intense and energetic precipitation known to the associated with auroral surges. As the substorm reaches recovery phase, the morphologies of the X-ray and visible/UV emissions diverge, with relatively more high energy X-rays emitted from the postmidnight sector primarily in two regions: one near 0000 MLT and one near 0600 MLT.

The total precipitating electron energy flux and mean electron energy calculated from the VIS, UVI, and PIXIE images are found to be in acceptable agreement (within $\sim$50%) in most regions. A temporal and spatial analysis of the observed high energy precipitation regions indicates that the precipitating high energy electrons at 0500–0800 MLT were injected at the time and location of the second substorm intensification and subsequently drifted, as has been found in previous studies. However, there are also high energy electrons observed continuously at 0000–0200 MLT for $\sim$30 min which persist into substorm recovery phase. For this substorm, their timing indicates that they originate in the substorm electron acceleration process, which must last for $\sim$30 min in order to continuously supply $\sim$100 keV precipitating electrons to this small local time range. Whether this process is similar in other substorms is a subject for further investigation.

These multispectral measurements highlight the fact that during a substorm, the visible/UV and X-ray emissions can be quite different and can be produced by precipitating electrons in significantly different energy ranges. This suggests that a remote measurement of the precipitating electron energy spectrum could be produced from a combination of low energy (visible or UV) and high energy (X-ray) emissions which may be more accurate than such a measurement from an individual imager.

Acknowledgments. This study was supported in part by NASA under contract NAG5-3170 at the University of Washington, contract NAS5-30316 at the University of Iowa, and contract NAS5-30372 at Lockheed Martin. S. A. Cummer was supported for this work by a National Research Council fellowship. Work at the University of Bergen was supported by the Norwegian Research Council.

References

Akasofu, S.-I., The development of the auroral substorm, *Planet. Space Sci., 12*, 273, 1964.

Anderson, P. C., D. L. Chenette, D. L. McKenzie, J. M. Quinn, M. Grande, and M. Carter, Energetic auroral electron distributions derived from global X-ray measurements and comparison with in-situ particle measurements, *Geophys. Res. Lett., 25*, 4105, 1998.

Codrescu, M. V., T. J. Fuller-Rowell, R. G. Roble, and D. S. Evans, Medium energy particle precipitation influences on the mesosphere and lower thermosphere, *J. Geophys. Res., 102*, 19977, 1997.

Craven, J. D., and L. A. Frank, The temporal evolution of a small auroral substorm as viewed from high altitudes with Dynamics Explorer 1, *Geophys. Res. Lett., 12*, 465, 1985.

Germany, G. A., M. R. Torr, D. G. Torr, and P. G. Richards, Use of FUV auroral emissions as diagnostic indicators, *J. Geophys. Res., 99*, 383, 1994.

Germany, G. A., G. K. Parks, M. Brittnacher, J. Cumnock, D. Lummerzheim, J. F. Spann, L. Chen, P. G. Richards, F. J. Rich, Remote determination of auroral energy characteristics during substorm activity, *Geophys. Res. Lett., 24*, 995, 1997.

Jentsch, V., Electron precipitation in the morning sector of the auroral zone, *J. Geophys. Res., 81*, 135, 1976.

Østgaard, N., J. Stadsnes, J. Bjordal, R. R. Vondrak, S. A. Cummer, D. Chenette, G. K. Parks. M. J. Brittnacher, and D. L. McKenzie, Global scale electron precipitation features seen in UV and X rays during substorms, *J. Geophys. Res., 104*, 10191, 1999a.

Østgaard, N., J. Stadsnes, J. Bjordal, R. R. Vondrak, S. A. Cummer, D. Chenette, M. Schulz, and J. Pronko, The cause of the localized maximum of X-ray emission in the morning sector—A comparison with electron measurements, *J. Geophys. Res.*, in review, 1999b.

Parrot, M., and C. A. Gaye, A statistical survey of ELF waves in a geostationary orbit, *Geophys. Res. Lett., 21*, 2463, 1994.

Rees, M. H., D. Lummerzheim, R. G. Roble, J. D. Winningham, J. D. Craven, and L. A. Frank, Auroral energy deposition rate, characteristic electron energy, and ionospheric parameters derived from Dynamics Explorer 1 images, *J. Geophys. Res., 93*, 12841, 1988.

Robinson, R. M., and R. R. Vondrak, Validation of techniques for space based remote sensing of auroral precipitation and its ionospheric effects, *Space Sci. Rev., 69*, 331, 1994.

Strickland, D. J., R. R. Meier, J. H. Hecht, and A. B. Christiansen, Deducing composition and incident electron spectra from ground-based auroral optical measurements: theory and model results, *J. Geophys. Res., 94*, 13527, 1989.

M. J. Brittnacher, G. K. Parks, Department of Geophysics, University of Washington, Seattle, WA 98195.

D. L. Chenette, Lockheed Martin Advanced Technology Center, Palo Alto, CA 94304.

S. A. Cummer, Department of Electrical and Computer Engineering, Duke University, Durham, NC 27708. (email: cummer@ee.duke.edu)

N. Østgaard, J. Stadsnes, J. Bjordal, Department of Physics, University of Bergen, N-5007 Bergen, Norway.

J. B. Sigwarth, L. A. Frank, Department of Physics and Astronomy, University of Iowa, Iowa City, IA 52242

R. R. Vondrak, NASA/Goddard Space Flight Center, Code 690, Greenbelt, MD 20771.

(Received September 17, 1999; revised December 2, 1999; accepted December 8, 1999.)